JOURNAL OF GEOPHYSICAL RESEARCH, VOL. 112, D22S04, doi:10.1029/2006JD007592, 2007

In situ measurements of trace gases and aerosol optical properties at a rural site in northern China during East Asian Study of Tropospheric Aerosols: An International Regional Experiment 2005

Can Li,[1] Lackson T. Marufu,[1] Russell R. Dickerson[1,2] Zhanqing Li,[1,3,4] Tianxue Wen,[5] Yuesi Wang,[5] Pucai Wang,[5] Hongbin Chen,[5] and Jeffrey W. Stehr[1]

Received 31 May 2006; revised 16 January 2007; accepted 15 February 2007; published 30 August 2007.

[1] In situ measurements of trace gases and aerosol optical properties were made in March 2005 at Xianghe (39.798°N, 116.958°E, 35 m), a rural site about 70 km southeast, and generally downwind of the Beijing metropolitan area. High pollutant levels were observed during the experiment, with CO (1.09 ± 1.02 ppmv, average ± standard deviation), SO_2 (17.8 ± 15.7 ppbv), NO_y (26.0 ± 24.0 ppbv), aerosol scattering coefficients (b_{sp}, (468 ± 472) × 10^{-6} m^{-1}), and aerosol absorption coefficients (b_{ap}, (65 ± 75) × 10^{-6} m^{-1}) all much higher than observed at some rural sites in the United States. O_3 (29.1 ± 16.5 ppbv) was relatively low during this study, suggesting inactive photochemical processes. Strong synoptic fluctuations in pollutant levels were detected every 4–5 days during the experiment, as cold fronts passing over the region drastically reduced the ground-level pollution. Very little precipitation was measured during the whole observational period, implying pollutant uplift and transport by rain-free cold fronts and dry convection. The single scattering albedo (SSA) observed (0.81 in the morning and 0.85 in the afternoon) indicates strongly absorbing aerosols near surface. The observed CO/SO_2 ratio (35.8) is higher than inventory values, but closer to the updated CO inventory of Streets et al. (2006) than to Streets et al. (2003) or Wang et al. (2005). The observed CO/NO_y ratio agrees better with inventories. Further analysis suggests that such comparisons may shed some light on the quality of emission inventories, but quantification of any error requires more extensive measurements over longer period and larger areas, as well as direct characterization of emission sources, especially mobile sources and small boilers. Using black carbon (BC)/CO ratio from the experiment, BC emissions from China are estimated at about 1300 Gg (10^9 g)/yr, but could be as high as 2600 Gg/yr.

Citation: Li, C., L. T. Marufu, R. R. Dickerson, Z. Li, T. Wen, Y. Wang, P. Wang, H. Chen, and J. W. Stehr (2007), In situ measurements of trace gases and aerosol optical properties at a rural site in northern China during East Asian Study of Tropospheric Aerosols: An International Regional Experiment 2005, *J. Geophys. Res.*, *112*, D22S04, doi:10.1029/2006JD007592.

1. Introduction

[2] The past two decades have seen tremendous economic growth in China as the nation with the world's largest population quickly emerges as a major player in the global economy. The continuous near-double-digit growth rate has been driven largely by expansion in industrial production. Accompanying the economic development is a rapid increase in energy consumption [*World Bank*, 2004], as well as emissions of atmospheric pollutants [*Streets and Waldhoff*, 2000]. Although certain efforts have been dedicated to emission control and environmental protection, these measures are often localized [e.g., *Beijing EPA*, 2002] and likely compensated for or overwhelmed by the overall growing trend, as has been seen from satellite measurements [*Richter et al.*, 2005]. Air pollution is severe and widespread in China; in 2002, only about one third of the 343 monitored cities met the Grade II National Ambient Air Quality Standard of China [*Hao and Wang*, 2005]. Primary and secondary atmospheric pollutants pose threats to human health and may cause thousands of excess deaths in China [*World Health Organization*, 2001]. Once lifted to higher altitudes and driven by strong westerly winds aloft, the pollution plume can travel over long distances [e.g., *Berntsen et al.*, 1999; *Jaffe et al.*, 1999, 2003; *Husar et al.*, 2001; *Prospero et al.*, 2003; *Allen et al.*, 2004; *Mari et al.*, 2004; *Guttikunda et al.*, 2005; *Wang et al.*, 2006], turning the local air pollution issue into a large-scale problem. There are also concerns that aerosols from China could change the patterns of regional

[1]Department of Atmospheric and Oceanic Science, University of Maryland, College Park, Maryland, USA.
[2]Also at Department of Chemistry and Biochemistry, University of Maryland, College Park, Maryland, USA.
[3]Also at Earth System Science Interdisciplinary Center, University of Maryland, College Park, Maryland, USA.
[4]Also at Institute of Atmospheric Physics, Chinese Academy of Sciences, Beijing, China.
[5]Institute of Atmospheric Physics, Chinese Academy of Sciences, Beijing, China.

0148-0227/07/2006JD007592$09.00

climate and hydrological cycles [e.g., *Xu*, 2001; *Menon et al.*, 2002; *Lau et al.*, 2005; *Huang et al.*, 2006].

[3] Several investigators [*Streets and Waldhoff*, 2000; *Streets et al.*, 2003, 2006; *Wang et al.*, 2005] have used "bottom-up" methods to compile local and regional emission inventories of pollutants such as CO, NO_x, and SO_2. These inventories have been tested with chemical transport models and available observations [e.g., *Tan et al.*, 2004; *Heald et al.*, 2004]. However, bottom-up inventories are limited by the availability and reliability of emission and energy use data. The fast but uneven development of the Chinese economy further complicates this issue. A wide variety of fuels and combustion technologies are currently used in different areas and economic sectors of China, making estimates of CO and BC emissions highly uncertain [e.g., *Streets et al.*, 2003; *Streets and Aunan*, 2005]. In recent years, several field campaigns have been carried out over the western Pacific region, downwind of the major emission sources of East Asia [e.g., *Hoell et al.*, 1997; *Jacob et al.*, 2003; *Huebert et al.*, 2003; *Parrish et al.*, 2004]. Combined with chemical transport model simulations, these field experiments provide not only evaluations of the inventory studies but also insights into the long-range transport mechanisms of pollutants emitted from this region [e.g., *Zhang et al.*, 2004]. Direct measurements of aerosols and precursor gases close to source regions are still insufficient for understanding, controlling, and mitigating the air pollution problem in East Asia. Chinese scientists and their international collaborators have made some progress in this regard, especially in the Beijing metropolitan area, where the 2008 Summer Olympic Games will be held [e.g., *Chan et al.*, 2005; *Sun et al.*, 2005; *Yang et al.*, 2005; *Zheng et al.*, 2005]. The complexity of emission sources in China, however, justifies simultaneous real-time measurements of both aerosols and major precursor gases.

[4] To characterize the emission, transport, and removal of atmospheric pollutants emitted from East Asia, particularly China, a U.S.-China joint Intensive Field Campaign (IFC) was conducted from February to April 2005 under the auspices of EAST-AIRE (East Asian Study of Tropospheric Aerosols: an International Regional Experiment). The major goals of EAST-AIRE are to understand better the origins, transport, physical, chemical, and optical properties of dominant natural and anthropogenic aerosols and gases, as well as to gain preliminary insights into the direct and indirect effects of these aerosols and gases on radiation, clouds, and precipitation. During this first IFC of EAST-AIRE, in situ measurements of aerosol optical properties, chemical composition and precursor gases were made from ground and aircraft.

[5] The ground-based experiment of the IFC was held at Xianghe in March 2005. This paper focuses on results acquired using the UMD instruments during the ground experiment. Results from the other instruments and the aircraft experiment are presented in companion papers [*Li et al.*, 2007; *Dickerson et al.*, 2007].

2. Methodology

2.1. Measurement Site

[6] The Xianghe Atmospheric Observatory (39.798°N, 116.958°E; 35 m above sea level) is located about 70 km southeast of the Beijing metropolitan area. This area of plains is surrounded by agricultural land, densely occupied residences and light industry. Sitting between two megacities (with Beijing to the northwest and Tianjin to the southeast) and less than 5 km west of the local town center (with a population of ~50,000), the site experiences frequent pollution plumes. Depending on the wind direction, instruments at the Xianghe site detect pollutants of urban, rural, or mixed origins. During the experiment, the area was generally cold and dry, with an average temperature of ~4.4°C and an average ambient relative humidity (RH) of ~36%. Very little precipitation (~0.1 mm in total) was observed during the experiment.

2.2. Instrumentation

2.2.1. Trace Gases

[7] O_3 was measured with a commercial instrument using UV absorption at 254 nm (Thermo Environmental Instruments Model 49, Franklin, Massachusetts). The instrument was calibrated with an in-house primary standard (Thermo Environmental Instruments Model 49 PS) before and after the field deployment. The instrument has a detection limit of 4 ppbv (signal-to-noise ratio S:N = 2:1 for $\pm 1\sigma$ noise) for 10-s data.

[8] CO data were collected using a modified [*Dickerson and Delany*, 1988] commercial nondispersive infrared gas filter correlation analyzer (Thermo Environmental Instruments Model 48). The instrument was calibrated with CO working standard gas (~1 ppmv CO in nitrogen Scott-Marrin Inc., Riverside, CA) traceable to a NIST (National Institute of Standards and Technology) standard reference material before and after the campaign. The instrument has a detection limit of 40 ppbv (signal-to-noise ratio S:N = 2:1 for $\pm 1\sigma$ noise), for 1-min means of 10-s data.

[9] SO_2 was measured using a modified [*Luke*, 1997] commercial detector, which utilizes pulsed UV fluorescence technology (Thermo Environmental Instruments Model 43C). The instrument was also calibrated with a NIST traceable standard material (~5 ppmv SO_2 in air, Scott-Marrin Inc., Riverside, CA) before and after the field deployment. For this research, the instrument has a detection limit of 80 pptv (signal-to-noise ratio S:N = 2:1 for $\pm 1\sigma$ noise) for 1-min means of 10-s data.

[10] A modified [*Fehsenfeld et al.*, 1987; *Stehr et al.*, 2000] commercial chemiluminescence detector (Thermo Environmental Instruments Model 42) was employed to measure NO and NO_y (total reactive oxides of nitrogen, $NO + NO_2 + NO_3 + 2 \times (N_2O_5) + HNO_3 + HONO + HNO_4 +$ peroxyacyl nitrates + organic nitrate) [*Seinfeld and Pandis*, 1998]. The instrument was calibrated with a working standard (~4.5 ppmv n-propylnitrate in nitrogen, and NO in nitrogen; Scott-Marrin Inc., Riverside, CA) before the field experiment. In China the instrument was calibrated with Chinese NO standards and via gas phase titration [e.g., *Dickerson et al.*, 1984]. The detection limit of the detector is 150 pptv (signal-to-noise ratio S:N = 2:1 for $\pm 1\sigma$ noise). The conversion efficiency for NO_2 exceeded 95% and was assumed unity for all NO_y compounds. The overall uncertainty of NO_y measurements using this technique is about ±30% [e.g., *Stehr et al.*, 2000].

[11] All the trace gas detectors were located in a room on the 3rd floor of the Xianghe site observatory building.

Sample flows were drawn from the top of the building (~15 m above ground) and directed into the detectors via Teflon sampling lines ~6 m in length. To protect the instruments, particle filters were installed ahead of the sampling lines for CO, SO_2, NO, and O_3. The filters were replaced after 10 days into the field experiment. Instrument readings immediately before and after the filter change did not show abrupt variations, suggesting that the sampling losses to the particle filters are probably within the uncertainties of the analytical techniques. Sampling losses to the sampling lines are likely less than 10%, as suggested by direct comparison with other instruments using much shorter sampling lines. Data were recorded with 1-min resolution and averaged into 10-min data.

2.2.2. Aerosol Optical Properties

[12] Information about aerosol absorption coefficients (b_{ap}) was acquired using a Particle/Soot Absorption Photometer (PSAP, Radiance Research, Seattle, WA). Used in a typical configuration, the instrument has a detection limit of 1.8×10^{-6} m^{-1} (signal-to-noise ratio S:N = 2:1 for $\pm 1\sigma$ noise) when using an average time of 1 min [*Bond et al.*, 1999]. Because of the high aerosol loadings experienced at Xianghe, we decreased the sampling flow rate from ~2 L/min to ~0.2 L/min to improve the filter change interval to a manageable level (once every 2–3 hours on a polluted day). The actual flow rate was calibrated with an electronic bubble flowmeter (DC-2, Bios International Corp., Butler, NJ). The influences of flow rate, spot size, and the interference from nonabsorbing aerosols were corrected following *Bond et al.* [1999]. The corrected aerosol absorption coefficients at 574 nm were extrapolated to 550 nm [*Virkkula et al.*, 2005]. We also assumed that the ambient RH had negligible effects on the absorption measurements, as RH was relatively low during the experiment. The uncertainty of the absorption measurement is about 30% at a 95% confidence level.

[13] An integrating nephelometer (TSI Model 3563, Shoreview, MN) was employed to measure aerosol scattering coefficients (b_{sp}) at three wavelengths. For an averaging interval of 5 min, the detection limits of the instrument at 450, 550, and 700 nm are 0.44×10^{-6} m^{-1}, 0.17×10^{-6} m^{-1}, and 0.26×10^{-6} m^{-1}, respectively (signal-to-noise ratio S:N = 2:1 [*Anderson et al.*, 1996]). The major source of uncertainty, especially when the sampled particles are dominated by coarse-mode particles, is the nonideal forward scattering truncation from 0 to ~7° [*Anderson et al.*, 1996]. Following *Anderson and Ogren* [1998], wavelength-dependent correction factors can be calculated for all three wavelengths by using the Ångström exponent (α) to represent changes of b_{sp} with wavelength. A measure of the wavelength-dependence of particle scattering, α is defined as:

$$\alpha = -\frac{\log\left[b_{sp}(\lambda_1)/b_{sp}(\lambda_2)\right]}{\log(\lambda_1/\lambda_2)}. \quad (1)$$

where $b_{sp}(\lambda_1)$ and $b_{sp}(\lambda_2)$ are the aerosol scattering coefficients at wavelengths λ_1 and λ_2, respectively. Aerosol scattering measurements using this instrument have an estimated uncertainty of ~10% [*Anderson et al.*, 1996]. The heat of the instrument reduces the RH below ambient values. The RH in the integrating volume of the nephelometer was 17.5% ± 17.5% ($\pm 2\sigma$) and never exceeded 42.5% during the experiment. The actual aerosol scattering in the atmosphere changes with environmental humidity and is often determined with the growth factor, an empirically derived relationship between b_{sp} and the environmental RH [*Charlson et al.*, 1992; *Jeong et al.*, 2007]. For this study, no correction of the humidity effect was performed because there is little information available concerning the aerosol growth factors in this area. The generally dry atmospheric conditions during the experiment kept the humidity effect to less than 20% for most of the time.

[14] For this experiment, the PSAP and the nephelometer were both deployed on top of the Xianghe site observatory building. Aerosol samples were drawn through straight conductive tubing of less than ~1 m before entering the instruments. No size-cut heads were used to limit the size range of the aerosol samples. Data from the PSAP and the nephelometer were recorded with a resolution of 1 and 5 min, respectively, and averaged over 10-min intervals.

2.3. Meteorological Data

[15] A 32-m meteorological tower located ~50 m southeast of the observatory provided automatic measurements of ambient temperature, relative humidity, and wind speed at five levels (2, 4, 8, 16, and 32 m above ground) every 10 min. A weather vane at the top of the tower determined the wind direction, and a barometer monitored local atmospheric pressure.

3. Results and Discussion

3.1. Pollutant Level

[16] Hourly averaged aerosol absorption coefficients at 550 nm and scattering coefficients at 450, 550, and 700 nm are shown in Figure 1. Also shown in the same plot are the locally observed temperature, relative humidity, surface pressure, wind direction, and wind speed. Hourly averaged trace gas (CO, SO_2, NO_y, and O_3) concentrations are presented in Figure 2. The gaps in both plots are due to a power failure (on 7 March, day of year (DOY) 66), routine maintenance of instruments, and instrument malfunctions. Heavy aerosol loadings at the site often saturated the PSAP's filter, and were responsible for the gaps in the aerosol absorption data in the early morning hours (0000–0700 local standard time (LST)). Figure 2 (first panel) also shows the aerosol optical thickness (AOT) at 500 nm determined with the colocated Cimel Sun photometer [*Li et al.*, 2007].

[17] The most prominent feature of air pollution at the Xianghe site, as revealed by Figures 1 and 2, is the very high concentration of pollutants for a nonurban site. Hereafter all results are presented as average ± standard deviation (σ) unless otherwise noted. The hourly averaged SO_2 concentration is 17.8 ± 15.7 ppbv, with a maximum 1-hour concentration of 96.5 ppbv. The hourly averaged CO concentration is 1.09 ± 1.02 ppmv, with a maximum 1-hour concentration of 6.59 ppmv. NO_y is more variable, with an hourly average concentration of 26.0 ± 24.0 ppbv and a maximum concentration of almost 184 ppbv. For comparison, the observations made at a rural site about

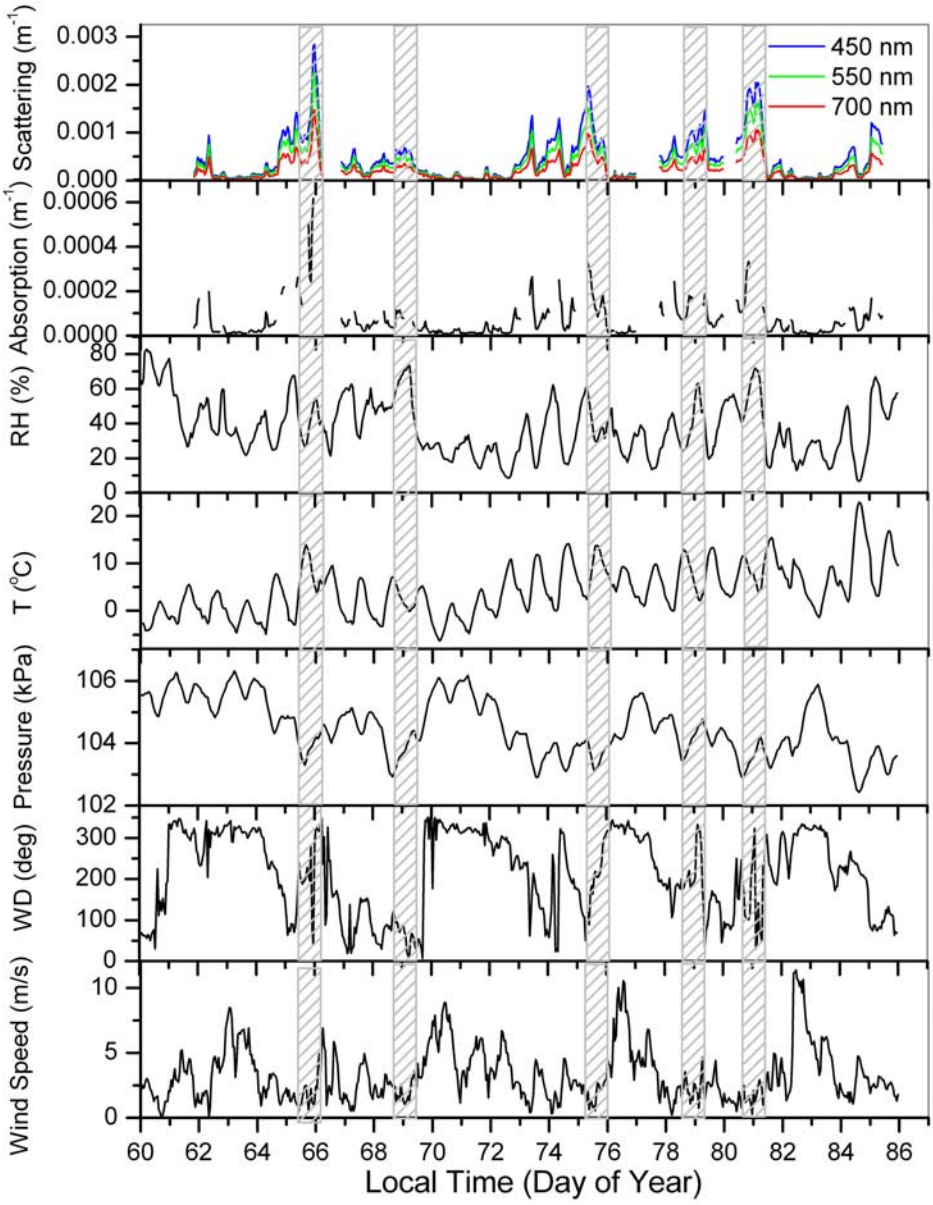

Figure 1. Hourly averaged aerosol scattering coefficients (450, 550, and 700 nm), aerosol absorption coefficients (550 nm), relative humidity (%), temperature (T, °C), surface pressure (kPa), wind direction (WD, degrees), and wind speed (m/s) observed at the Xianghe site from 2 to 26 March 2005. Time periods with analyzed cold front passages are approximated with hatched areas.

50–60 km east of the urban center of Baltimore, MD, USA indicate less SO_2 (2.8 ± 3.2 ppbv), CO (0.219 ± 0.087 ppmv), and NO_y (8.1 ± 6.3 ppbv) [*Stehr et al.*, 2000]. The very high aerosol loadings at the Xianghe site are evident in the scattering and the absorption data. The aerosol scattering coefficients at 550 nm, as measured by the nephelometer, were $(468 \pm 472) \times 10^{-6}$ m^{-1}, while the PSAP measurements suggested that the aerosol absorption coefficients at the same wavelength were $(65 \pm 75) \times 10^{-6}$ m^{-1}. Using the same type of instruments (TSI 3563 nephelometer and Radiance Research PSAP), *Delene and Ogren* [2002] measured aerosol properties at Bondville, IL, USA, an anthropogenically influenced continental site located at a similar latitude. The annually averaged aerosol scattering ($(57.7 \pm 17.7) \times 10^{-6}$ m^{-1}) and absorption ($(4.66 \pm 2.27) \times 10^{-6}$ m^{-1}) coefficients at Bondville were almost an order of magnitude lower than at Xianghe. Aerosol loadings at Bondville were lower in March than in other months [*Delene and Ogren*, 2002]. The ambient temperatures and solar flux during spring at Xianghe were too low to be conducive to the photochemical production of O_3, and the concentration of this secondary pollutant was not very high (29.1 ± 16.5 ppbv) during the experiment, with an hourly maximum of 73.4 ppbv.

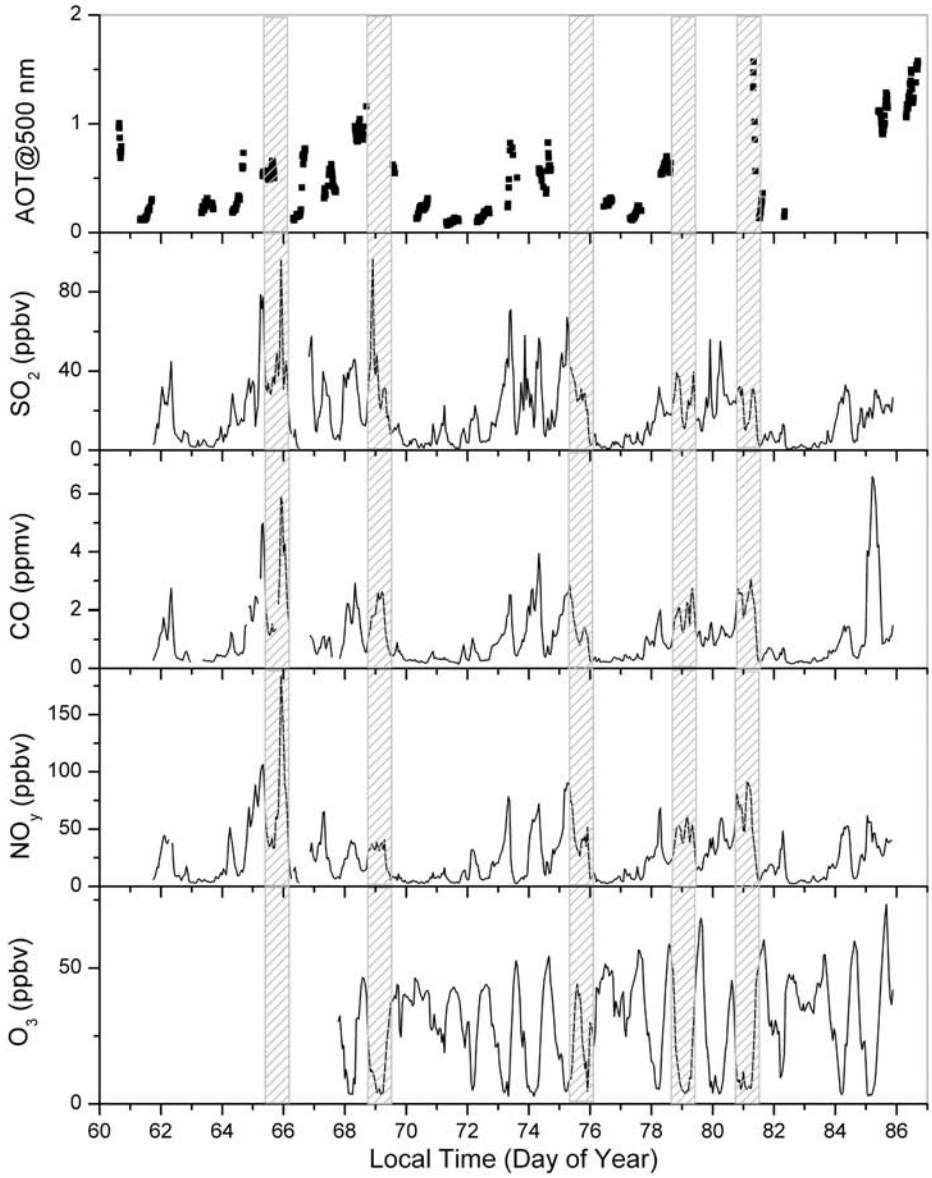

Figure 2. Hourly averaged concentrations of SO_2, CO, NO_y, and O_3 observed at the Xianghe site from 2 to 26 March 2005. Time periods with analyzed cold front passages are approximated with hatched areas. The first panel shows the aerosol optical thickness (at 500 nm) determined with the colocated Cimel Sun photometer.

[18] During the TRACE-P and ACE-Asia field campaign in the spring of 2001, *Wang et al.* [2004] observed high levels of pollutants at a rural site in eastern China. Their reported CO (677 ppbv), SO_2 (15.9 ppbv), and NO_y (13.8 ppbv) concentrations were lower than but comparable to those observed at Xianghe. Such high pollutant concentrations observed at different rural sites in China probably reflect the large extent of air pollution issues in China.

3.2. Temporal Variability

[19] As can be seen from Figure 2, overall, SO_2 and NO_y concentrations decreased during the experiment, while O_3 concentration on the other hand, increased over the observation period. These changes probably reflect the seasonal trends of air pollution at Xianghe, as March is the month of transition from late winter to early spring in northern China. Increasing ambient temperatures (Figure 1) and deepening planetary boundary layer (PBL) could facilitate the dispersion of atmospheric pollutants, and decrease the primary pollutant concentrations near the ground. The causes of the SO_2 and NO_y decreases are probably two-fold. Besides the changes in meteorological conditions, intensities of emission sources also change with season. One example is increase in ambient temperature would reduce the demand for heating and the associated combustion activities. The increase in O_3 levels reflects accelerated photochemical

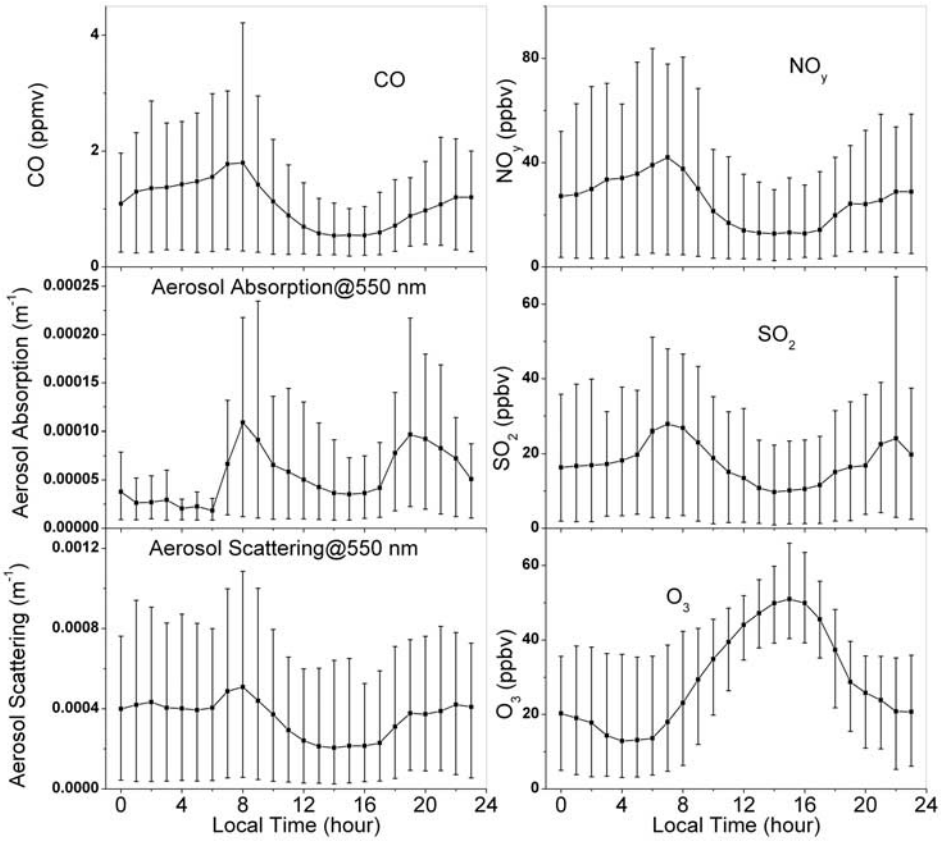

Figure 3. Diurnal cycles of CO, NO_y, aerosol absorption coefficients (550 nm), SO_2, aerosol scattering coefficients (550 nm), and O_3 at the Xianghe site from 2 to 26 March 2005. Error bars are 10th (lower bars) and 90th (upper bars) percentiles of the data.

production as ambient temperature gets higher and solar irradiation becomes stronger, although O_3 concentration remained relatively low throughout the whole experiment. CO does not show an apparent overall trend in Figure 2. A substantial peak in CO concentration is seen during the last few days of this field experiment. We attribute this to the onset of agricultural activities in this region in the last a few days of the experiment. From 20 to 26 March (DOY 79–85), the authors observed biomass burning (clearing of agricultural land) around the site, which is an important source of atmospheric CO [*Crutzen and Andreae*, 1990] but less important for SO_2. 20 March 2005 is the vernal equinox in the Chinese lunar calendar, an important date in traditional Chinese agricultural guides. Much higher CO/NO_y and CO/SO_2 ratios were often detected during these biomass burning events. A detailed description of a major burning case is given in section 3.3.1. Aerosol optical properties do not show an obvious seasonal trend, probably because of our relatively short record. Also, different aerosol sources could change differently over time. For example, emissions from heating could reduce while dust and biomass burning emissions could increase during the experiment.

[20] Fast transitions between highly polluted and relatively clean episodes are seen in Figures 1 and 2. AOT, measured by the Cimel Sun photometer deployed at the same location, also shows dramatic fluctuations for the same period [*Li et al.*, 2007]. Surface weather analyses (Korean Meteorological Administration: available online at http://abc-gosan.snu.ac.kr/sfc.html) identify five cold-front passages on 5–6 March (DOY 64–65), 10–11 March (DOY 69–70), 16–17 March (DOY 75–76), 19–20 March (DOY 78–79), and 21–22 March (DOY 80–81). These frontal passages were accompanied by abrupt changes in local wind direction (often from south to west or northwest), increases in atmospheric pressure and decreases in ambient temperature as well as humidity.

[21] The third through seventh panels of Figure 1 present the hourly averaged temperature, relative humidity, local surface pressure, wind direction, and wind speed during the experiment. Shaded areas in Figures 1 and 2 indicate cold front passages. Aerosol absorption and scattering coefficients, NO_y, SO_2, and CO concentrations all suggest pollutant accumulation before cold front passages and quick dissipation after cold front passages, as the continental tropical air mass is replaced by continental polar air mass. High wind speeds behind cold fronts often promote the ventilation and vertical mixing of pollutants, leading to decreased surface concentrations. Descending air from less populated and less industrialized northern regions (Mongolia and Siberia) might also contribute to the low pollutant levels associated with these incoming high-

pressure systems. One study on the seasonal changes of fine particles ($PM_{2.5}$) in Beijing found lower $PM_{2.5}$ concentrations in winter [*Zheng et al.*, 2005] when frontal activity is most intense and photochemical production of secondary particles is least active. This is consistent with the AOT observations made at Xianghe [*Li et al.*, 2007]. The O_3 concentration, on the other hand, shows increased mixing ratios during the morning hours (~40 ppbv instead of a few ppbv under normal conditions) behind cold fronts. This fairly high O_3 level is often accompanied by low concentrations of pollutants such as CO (a few hundred ppbv), SO_2 (a few ppbv) and NO_y (a few ppbv), implying reduced titration of O_3 by local pollutants. Higher wind speeds behind cold fronts dilute primary pollutants and increase the thickness of nocturnal PBL, thus making O_3 loss at night less efficient.

[22] Diurnal cycles of pollutants (Figures 1 and 2) show that aerosol absorption and scattering coefficients, as well as CO, SO_2, and NO_y concentrations all have maxima during the local morning rush hour and minima during the local afternoon hours. O_3 concentration has an opposite phase, with maxima in the afternoons and minima in the mornings. Using all available 10-min data, we calculated the average diurnal variation of CO, NO_y, SO_2, and O_3, aerosol scattering and absorption at 550 nm for each hour of the day (Figure 3). The error bars shown on the same plot are 10th (lower bars) and 90th (upper bars) percentiles of the data. Except for O_3, all the other parameters show minima at around 1500 LST and accumulate gradually until reaching maxima during the local rush hour on the following day. Both meteorological conditions and emission activities contribute to these diurnal cycles. The generally cold and dry conditions during the experiment often lead to the formation of nocturnal inversion close to ground level. The dispersion of pollutants emitted from the ground level is inhibited until the following morning when solar radiation destroys the nocturnal inversion. Local temperature measurements suggest that the inversion breaks up around 0800 LST (data available online at the EAST-AIRE website: http://www.atmos.umd.edu/~yuan/web_proj/data/arm/china/xianghe/tower/). Besides the meteorological factors, stronger emissions during the morning rush hour may also enhance the peak pollutant levels in the morning. *Wang et al.* [2005] suggested that a common practice among the rural households in northern China is to set up fires in stoves in the early morning and the late afternoon for cooking and heating. In addition, small factories around the site start business around 0800 LST. As the ambient temperature increases during the day, convection due to solar heating picks up and forms the unstable daytime PBL. Stronger surface winds and active convection during daylight hours dilute pollutants near the ground. Higher temperatures at noon also reduce the needs for heating and the associated emissions.

[23] The error bars in Figure 3 show that CO, NO_y, SO_2, and aerosol scattering coefficients are more variable in the morning and evening than at midday. The sampling sizes for these parameters are similar for each hour of the day. Taking CO as an example, we have 120 and 122 data points (10-min averages) for 0700–0800 and 1500–1600 (LST), respectively. So the diurnal change in pollutant variability probably reflects the different emission sources detected by the instruments at different times of the day. The chemical characteristics of the local emission sources are diverse; during the experiment, we observed coal-fueled boilers, two-stroke, four-stroke and diesel-powered vehicles, biofuel, liquefied propane and agricultural burning within 5 km of the site. During the morning and evening hours, the instruments at Xianghe get more signals from nearby emission sources, as wind speeds are relatively low and atmospheric mixing is relatively weak. Consequently the measured plumes are variable at these times. During the daytime, stronger mixing and higher wind speeds help transport mixed plumes from a larger region to the site, and reduced variability is seen at noon and in the early afternoon. Data from different times of the day can therefore be used to characterize emission sources of different regions. The variability of the aerosol absorption coefficients cannot be properly determined between 2300 and 0700 LST because of the gaps in the PSAP data due to the filter saturation problem mentioned above.

3.3. Pollutant Ratios

[24] Different types of emissions sources often have distinct emission profiles. For instance, a boiler used in electricity generation has a high flame temperature and excess air supply. Such boilers emit a lot of NO_x but little CO. On the other hand, a coal-burning stove for household heating usually has a lower flame temperature and limited ventilation. As a result, the emission of NO_x is suppressed and the emission of CO is intense. Simultaneous measurements of NO_x and CO can help characterize the emission sources. Once emitted into atmosphere, NO reacts and transforms rather quickly, so for this study the ratio between CO and NO_y is used.

[25] The ratios of CO/NO_y, CO/SO_2, b_{sp}/SO_2, and b_{sp}/b_{ap} during the morning rush hour (0700–0900 LST) and midday (1400–1600 LST) were calculated via correlation analysis of simultaneous measurements. As shown in Figure 4, the correlation coefficients for CO/NO_y, CO/SO_2, b_{sp}/SO_2, and b_{sp}/b_{ap} are much higher in the afternoon than during the morning rush hour. This supports the argument that the afternoon data have information from better mixed and more "regional" plumes, while the early morning data contain information from less mixed and more "local" plumes. Table 1 summarizes the results of the correlation analysis.

3.3.1. CO/NO_y and CO/SO_2 Ratios

[26] The CO/NO_y ratio is 35.4 for the morning data and 27.2 for the afternoon data, implying higher relative contribution from high-temperature combustion sources for the larger region. More industrialized cities in China have more of high-temperature combustion sources, whereas rural areas have more of low-temperature sources such as residential stoves burning biofuel or coal. Thus plumes from the large point sources in the region contribute to the lower CO/NO_y ratio in the more regional afternoon data. Local small factories could be another factor, as they often use small-scale boilers (~1 MW) in production, and run during daytime. Those boilers are usually operated with substantial flame temperatures and excess air supply (D. Zhou, personal communication, 2005), emitting plumes with a relatively low CO/NO_x ratio.

[27] The correlation coefficient between CO and SO_2 is slightly higher than that between CO and NO_y, even

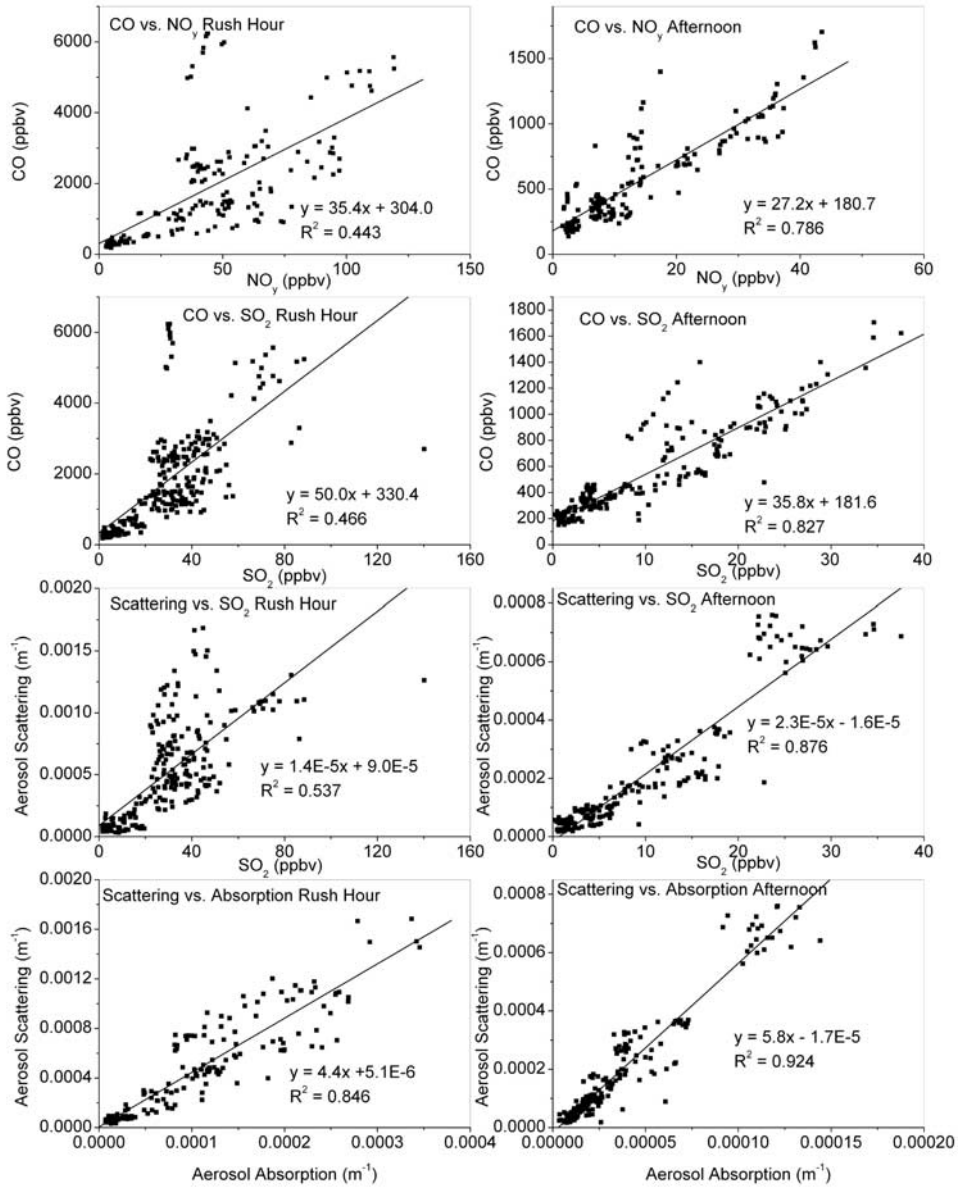

Figure 4. Correlations of CO and NO_y, CO and SO_2, aerosol scattering coefficients (550 nm) and SO_2, aerosol scattering coefficients (550 nm) and aerosol absorption coefficients (550 nm) during (left) the morning rush hour (0700–0900 LST) and (right) the midafternoon (1400–1600 LST) at the Xianghe site from 2 to 26 March 2005. All data points are 10-min averages. The equations shown in the plots are the best fit lines through the data.

when sulfate aerosols are not considered in the correlation analysis. This might reflect the fact that CO and SO_2 have more emission sources in common than CO and NO_y. Coal is the dominant energy source in China and is widely used in the North for household heating and cooking. *He and Chen* [2002] reported that the sulfur content of coal in China is 1.1–1.2% by weight on average, but can be as high as 3%. Low-efficiency stoves burning sulfur-containing coal emit both SO_2 and CO in substantial amounts. Besides being an important energy source for the residential sector,

Table 1. Results of the Correlation Analysis

	CO/NO_y		CO/SO_2		b_{sp}/SO_2[a]		b_{sp}/b_{ap}	
	AM	PM	AM	PM	AM	PM	AM	PM
Slope	35.4	27.2	50.0	35.8	1.4×10^{-5}	2.3×10^{-5}	4.4	5.8
y-intercept	304.0	180.7	330.4	181.6	9.0×10^{-5}	-1.6×10^{-5}	5.1×10^{-6}	-1.7×10^{-5}
R^2	0.44	0.79	0.47	0.83	0.54	0.88	0.85	0.92

[a]Unit is m^{-1}/ppbv.

coal is also used in large quantities for electricity generation and industrial production. These high-efficiency combustion activities are likely to be important sources of SO_2 but not CO. The CO/SO_2 ratio in more "regional" signals (35.8) is lower than that in more "local" signals (~50.0), reflecting the difference in source composition.

[28] Compared to other studies, the y-intercepts of the afternoon CO/NO_y and CO/SO_2 scatterplots are about 180 ppbv, close to the midlatitude continental background [*Novelli et al.*, 1998]. The slopes (CO/NO_y and CO/SO_2 ratios) of the afternoon scatterplots are similar to those observed at a rural site in Eastern China (CO/NO_y: 35 versus 37; CO/SO_2: 36 versus 29, the latter values are from *Wang et al.* [2002, 2004]).

[29] The CO/NO_y and CO/SO_2 ratios also helped to identify a major agricultural burning event. On 26 March (DOY 85) CO concentrations as high as 7 ppmv were observed at the Xianghe site while NO_y (~40 ppbv) and SO_2 (~25 ppbv) levels did not increase. Agricultural burns are characterized by high CO/NO_y ratios [e.g., *Wang et al.*, 2002; *Streets et al.*, 2003]. Through an emission profile study, *Zhang et al.* [1999] found that SO_2 emissions from crop residue combustion were rather low in this area. CO and NO_y were fairly well correlated ($R^2 = 0.568$) during this high-CO event, with a CO/NO_y ratio of ~125. The CO/SO_2 ratio was also very high (~250), although the correlation was not as good. The observed CO/NO_y and CO/SO_2 ratios were similar to the values estimated for biomass burning emissions [*Crutzen and Andreae*, 1990], reflecting the biomass burning origin of the plume. Compared to published emission factors for agricultural waste burning [*Andreae and Merlet*, 2001], the observed BC and NO_y concentrations were relatively low (BC/CO mass concentration ratio: $\sim 1.3 \times 10^{-3}$ (this study) versus 7.5×10^{-3} [*Andreae and Merlet*, 2001]; CO/NO_y ratio: ~125 (this study) versus 39 [*Andreae and Merlet*, 2001]), suggesting smoldering processes.

3.3.2. The b_{sp}/SO_2 and b_{sp}/b_{ap} Ratios

[30] Aerosol scattering coefficients are fairly well correlated with SO_2 concentration. As has been demonstrated by aerosol chemical composition studies at rural and urban sites in this region [e.g., *He et al.*, 2001; *Zheng et al.*, 2005; *Sun et al.*, 2005], sulfate is one of the most important aerosol compounds in northern China. The b_{sp}/SO_2 ratio is ~50% higher in the afternoon than in the morning, probably reflecting aging of primary pollutants. Also the relative role of organic aerosols is probably higher in the morning when emissions from vehicles and biofuel burning are more important. The strong mixing within the daytime PBL might also contribute to the higher b_{sp}/SO_2 ratio observed in the afternoon. Once the nocturnal inversion is destroyed, "yesterday's pollutants" remaining in the residual layer (the layer above the shallow nocturnal boundary layer) are then brought down to the ground level by large eddies. The pollutants from the residual layer are often of greater chemical age [e.g., *Taubman et al.*, 2004] and more thoroughly reacted. Lack of vertical profiles of pollutants complicates further investigation of this mechanism.

[31] The b_{sp}/b_{ap} ratio is slightly higher in the afternoon than in the morning. This could be explained with BC emitted from a large number of low-efficiency stoves in the rural areas surrounding the Xianghe site. The chemical aging processes, which convert precursor gases into nonabsorbing aerosols (e.g., sulfate and nitrate), also contribute to the higher b_{sp}/b_{ap} ratio observed in the afternoon as freshly emitted gas phase pollutants transform over time. Aged aerosols in the residual layer are often "brighter" (more scattering). The single scattering albedo (SSA), a critical parameter in aerosol radiative forcing research, is defined as the ratio between aerosol scattering and aerosol extinction (scattering + absorption). If we use the b_{sp}/b_{ap} ratios (the slopes of the best fit lines in Figure 4) obtained here to calculate SSA for the morning and afternoon hours (neglecting the rather small intercepts in the fits), SSA at 550 nm would be near 0.81 in the morning and around 0.85 in the afternoon. For comparison, SSA retrieved with the colocated Cimel Sun photometer was about 0.9 during the same period [*Li et al.*, 2007]. The difference originates presumably from the different aerosols actually detected by the two instruments, since the Cimel retrieval is sensitive to aerosols in the whole atmospheric column, while the PSAP and nephelometer measure surface values. Compared to the other surface measurements in China, SSA derived from this experiment is lower than that determined in the Yangtze delta region (0.93 [*Xu et al.*, 2002, 2003]), but similar to that in Guangzhou (0.86 [*Andreae et al.*, 2005]) and Beijing (0.81 [*Bergin et al.*, 2001]). Overall, currently available measurements all suggest strong absorbing properties of aerosols in the eastern part of China.

3.4. Implications for Emission Inventories

3.4.1. CO and SO_2 Emissions

[32] Comparing the observed pollutant ratios to the estimated ratios from inventory studies provides an evaluation of the inventories. Observations made at a rural site in Eastern China [*Wang et al.*, 2002, 2004] suggest possible underestimation of CO emitted from China by *Streets et al.* [2003]. A number of models [e.g., *Carmichael et al.*, 2003; *Tan et al.*, 2004] have also been employed to investigate the "missing" CO sources in China. A recent CO emission inventory [*Streets et al.*, 2006] increases CO emissions from China by 36%, reducing the discrepancies between observations and inventory estimates. Here we further examine emission inventories for China, by contrasting the observed CO/SO_2 and CO/NO_y ratios from this study to inventory values.

[33] Table 2 lists the CO/SO_2 and CO/NO_x (CO/NO_y) ratios from this study, an experiment carried out at street level in downtown Beijing (T. Wen et al., Trace gases and aerosol observations in Beijing: 1. Evaluations of emission inventories, manuscript in preparation, 2007, hereinafter referred to as Wen et al., manuscript in preparation, 2007), an inventory study covering East Asia [*Streets et al.*, 2003], an updated CO emission inventory for China after TRACE-P field campaign [*Streets et al.*, 2006], and a high-resolution inventory for a region in eastern China including Xianghe [*Wang et al.*, 2005]. To reflect the characteristics of air pollution for the larger region, afternoon ratios from this experiment are compared to results from the other studies. The different ratios between the two experimental studies could be explained with the different sources represented by the two sites. Measurements made in downtown Beijing are subject to large influences from mobile sources, which emit both CO and NO_x, but with a

Table 2. Observed and National Inventory Pollutant Ratios[a]

	This Study	Wen et al. (Manuscript in Preparation, 2007)	*Streets et al.* [2003]	*Streets et al.* [2006][b]	*Wang et al.* [2005][c]
CO/SO_2	35.8	72.1	13.0	17.5	7.7
CO/NO_x	27.2	25.4	16.7	22.7	8.6

[a]Unit is ppbv/ppbv.
[b]Use SO_2 and NO_x emission data from *Streets et al.* [2003].
[c]Emission inventory is regional.

lower CO/NO_x ratio than residential sources [*Wang et al.*, 2005]. Therefore Wen et al. (manuscript in preparation, 2007) observed a slightly lower CO/NO_x ratio than this study. The CO/SO_2 ratio observed in Beijing is higher than the Xianghe observations, since mobile sources emit little SO_2. Also, high-sulfur coal has been gradually replaced by low-sulfur coal and other cleaner fuels in Beijing since 1998, as part of the government's efforts to improve air quality [*Brajer and Mead*, 2003]. Despite the differences shown above, observational studies at rural and urban sites both show higher CO/SO_2 ratios than the inventories. CO/SO_2 ratio derived from our experiment is a factor of three higher than *Streets et al.* [2003] and a factor of four higher than *Wang et al.* [2005]. The large discrepancy between our observations and these two earlier inventory studies [*Streets et al.*, 2003; *Wang et al.*, 2005] implies that these inventory studies might underestimate CO emissions from China, as SO_2 emission estimates are considered more robust than those for CO [*Streets et al.*, 2003]. It is also possible that SO_2 emissions are overestimated, as the NO_y/SO_2 ratio from this experiment ($\sim$1.18) is about 40% higher than the inventories (0.78 [*Streets et al.*, 2003] and 0.89 [*Wang et al.*, 2005]). Another possibility is SO_2 emissions from China have decreased from 2000 to 2005. However, low-sulfur fuels have been replacing high-sulfur coal in the urban area of Beijing in recent years, but not in rural areas like Xianghe and smaller cities/towns. With a 36% increase in CO emissions from China, the new CO emission inventory by *Streets et al.* [2006] gives a higher CO/SO_2 ratio, which is still only half of our observations. However, quantitatively evaluating emission inventories with our current observations is difficult, because of a number of uncertainty sources. Different spatial coverage of bottom-up inventories and in situ measurements is one of the issues, as the inventory studies cover a relatively large region (national or regional), but measurements may largely reflect the properties of nearby emission sources. In section 3.4.2, we discuss the spatial issue of the inventory evaluation. Some other issues are discussed in section 3.4.3.

3.4.2. Cluster Analysis and Implications for Regional Emission Inventory

[34] Figure 5 presents the inventory ratios of CO/SO_2 and CO/NO_y for March 2001, calculated using the updated CO emission inventory by *Streets et al.* [2006] and their earlier estimates of SO_2 and NO_x emissions for the same period [*Streets et al.*, 2003]. The $0.5 \times 0.5^\circ$ grids shown in Figure 5 are grids with at least 10000 tons of estimated CO emissions (The Xianghe grid, 39.5–40°N, 116.5–117°E, is estimated to emit about 30000 tons of CO in March 2001). For a clearer view of the spatial pattern of inventory pollutant ratios, we set 50 as the upper limit of the color scale in Figure 5; but some grids shown in the plot have CO/SO_2 and/or CO/NO_y inventory ratios higher than 50. The blue and red lines in Figure 5 (top) are 24-hour backward trajectories during our experiment, calculated using the NOAA Air Resource Lab (ARL) HYSPLIT model [*Draxler and Rolph*, 2003] and NCEP reanalysis meteorological data. All trajectories are started at 1500 LST, 500 m above ground level. They could be separated into two groups, one with flows from west and southwest and often relatively polluted (red lines: DOY 65, 68, 73–75, 78, 80, and 85), and the other group with flows from north and northwest and sometimes relatively clean (blue lines: DOY 61–64, 66–67, 69–72, 76–77, 79, and 81–84). A few trajectories passing over the grid of metropolitan Beijing (39.5–40°N, 116–116.5°E) are marked in green in Figure 5 (bottom) (DOY 65, 74–75, 78, and 80).

[35] The CO/SO_2 inventory ratios show an obvious spatial pattern over the region around Xianghe, with the CO/SO_2 inventory ratios in the north (higher than 45) more than twice as high as ratios in the south (around 20). The CO/SO_2 ratio for the Beijing grid is even lower at about 12.5, while the same ratio for the Xianghe grid is around 22.4. CO/NO_y (NO_x) inventory ratios have a different spatial pattern, with the Beijing grid and the area southeast of Xianghe showing lower CO/NO_y ratios. Table 3 summarizes the pollutant inventory ratios for areas north and northwest of Xianghe, west and southwest of Xianghe, the Beijing grid, and the Xianghe grid. Results of correlation analysis for different trajectory groups are summarized in Table 4.

[36] When air comes from north or northwest of Xianghe (blue lines, Figure 5, top), SO_2, NO_y and CO are not well correlated, suggesting air parcels with different chemical ages or emission sources. Under certain conditions, descending flows from north or northwest bring relatively clean air with CO concentrations close to background level ($\sim$200 ppbv) and very low SO_2 and NO_y. Under stagnant conditions, we may detect fresh plumes with $\sim$1 ppmv of CO from the same direction, sometimes with a biomass burning signature. On the afternoon of 20 March (DOY 79), we observed $\sim$1 ppmv of CO with $\sim$10 ppbv of SO_2 and NO_y, probably associated with agricultural burnings in the area. Such diverse conditions complicate the direct comparison between emission inventories and measurements. The measurement-derived CO/SO_2 ratio of 33 is lower than the inventory ratio (57), but the observed CO/NO_y ratio (41) is close to the inventory value (35). The high CO/SO_2 inventory ratios in the region are attributed to traffic sources, which contribute to more than 70% of total CO emissions in the area according to *Streets et al.* [2006], even for the mountainous grids of 40.5–41°N, 116–117°E. CO emissions from the traffic sources in these two $0.5 \times 0.5^\circ$ grids are estimated to be about 310000 ton in 2001, only slightly lower than the traffic emissions from the Beijing grid (386000 ton in 2001) [*Streets et al.*, 2006]. Reexamining mobile sources in China is called for to reduce the uncertainties revealed here.

[37] CO, SO_2 and NO_y are well correlated for air from west and southwest of Xianghe (red lines, Figure 5, top). CO/SO_2 ratio derived for these trajectories (36.7) are similar to the ratio derived from all afternoon measurements

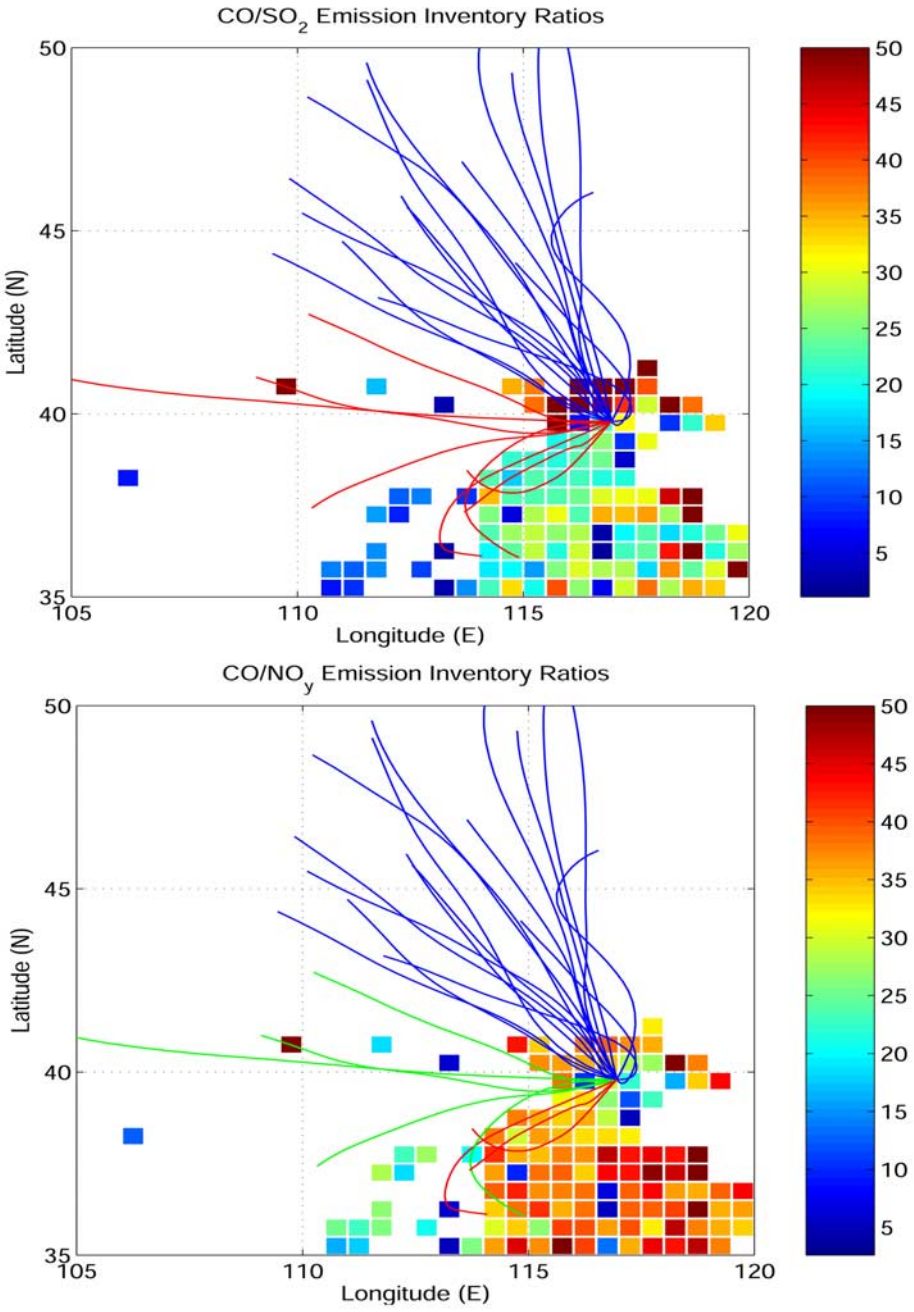

Figure 5. Emission inventory ratios of (top) CO/SO_2 and (bottom) CO/NO_x in March 2001 [*Streets et al.*, 2003, 2006]. Only grids with CO emissions of 10000 ton/month or higher are shown. The upper limit of color scale is set at 50 for clearer view of the spatial patterns, although some grids shown have ratios higher than 50. Blue, red and green lines are 24-hour backward trajectories started at 1500 LST, 500 m above ground over Xianghe, calculated with HYSPLIT model and NCEP global reanalysis data. Blue lines, red lines (Figure 5, top), and green lines (Figure 5, bottom) represent trajectories passing over areas with high CO/SO_2 inventory ratio, low CO/SO_2 inventory ratio, and the grid of Beijing, respectively.

(Figure 4), and more than a factor of two higher than the averaged inventory value for the area west and southwest of Xianghe (Table 3). Also the y-intercept of about 170 ppbv is close to background CO concentration. For CO/NO_y ratio, the observed value (21.8) is not far from the inventory value of 24.0, although the y-intercept is more than 300 ppbv. To reduce the influences of local emission sources, we also calculated the CO/SO_2 ratio under higher wind speed, after removing the data collected when local wind speed was lower than 3 m/s. The R^2 (0.656) and y-intercept (138.5 ppbv) become lower for the high-wind-speed-only data, but CO/SO_2 ratio remains almost the same (38.6). We also noticed that a couple of trajectories might have passed over a grid about 600 km west of Xianghe, where CO

Table 3. Regional Inventory Pollutant Ratios Within Different Areas Around Xianghe[a]

			Streets et al. [2003]		*Streets et al.* [2006][b]	
Area	Latitude Range	Longitude Range	CO/SO_2	CO/NO_x	CO/SO_2	CO/NO_x
N and NW	40–41°N	114.5–117.5°E	45.7	28.2	57.2	35.3
W and SW	37.5–40°N	114–117°E	10.1	14.7	16.5	24.0
Beijing	39.5–40°N	116–116.5°E	10.9	16.3	12.5	18.7
Xianghe	39.5–40°N	116.5–117°E	15.0	19.1	22.4	28.6

[a]Unit is ppbv/ppbv.
[b]Use SO_2 and NO_x emission data from *Streets et al.* [2003].

emitted from the large steel mills in the city of Baotou could possibly transport over long distances and influence our measurements. However, with the data from those two trajectories ignored, the CO/SO_2 ratio derived for the rest of west/southwest trajectories is still 35.6, with a R^2 of 0.752 and a y-intercept of 192.9 ppbv. So the CO/SO_2 correlation analysis for air from west and southwest consistently suggests a CO/SO_2 ratio more than 100% higher than the inventory value, lending us some confidence concluding that CO emissions might be underestimated or SO_2 emissions might be overestimated for the area west/southwest of Xianghe.

[38] For the trajectories passing over the Beijing grid, the CO/SO_2 ratio (41.4) derived from our measurements is not as high as the observations made in downtown area (Table 2) (Wen et al., manuscript in preparation, 2007), but still a factor of three higher than the inventory ratio for the Beijing grid (12.5). The grid west of metropolitan Beijing (39.5–40°N, 115.5–116°E) has higher CO/SO_2 ratio, but its CO emission is only one fifth that of the Beijing grid. Our CO/NO_y ratio from this trajectory group (36.5) is higher than Wen et al. (manuscript in preparation, 2007), and is twice as high as the corresponding inventory ratio (18.7). CO, SO_2, and NO_x are regularly monitored by Beijing EPA at sites mostly located in downtown Beijing, CO/SO_2 and CO/NO_x ratios calculated from annual average concentrations during 2000–2004 are 89 and 56, respectively (T. Wen, personal communication, 2006). These ratios could be biased high, however, as SO_2 and NO_x would be removed through fast photochemical processes in summer months. The CO/SO_2 inventory ratio for the grid north of the Beijing grid (40–40.5°N, 116–116.5°E) is much higher (Figure 5) than the Beijing grid, with strong traffic CO emissions comparable to the Beijing grid. This is probably true as the area north of metropolitan Beijing has been under fast development and urbanization over recent years. However, even after integrating the inventory emissions from these two grids (i.e., consider the area of 39.5–40.5°N, 116–116.5°E as the urbanized area of Beijing), the inventory CO/SO_2 (17.0) and CO/NO_y (22.3) ratios are still considerably lower than observations. Thus it seems plausible that for the urban area of Beijing, CO emissions are underestimated (or SO_2 emissions are overestimated) by inventory studies. Detailed analysis of pollutant emissions in downtown Beijing is given by Wen et al. (manuscript in preparation, 2007). It is worth noting that current emission inventories [*Streets et al.*, 2003, 2006] tend to give rather low CO/SO_2 (NO_x) ratios for big cities in China such as Beijing, Tianjin (Figure 5, 39–39.5°N, 117–117.5°E), Shanghai, and Guangzhou. Characterizing emissions from mobile sources or small-scale boilers [*Streets et al.*, 2006] may help reduce the uncertainties in emission inventories for big cities in China.

3.4.3. Other Issues of Inventory Evaluation

[39] Besides the spatial issue discussed above, some other issues could further complicate the comparison between inventories and measurements. Measurements are normally only available for a limited period of time, whereas emission inventories are often based on annual activity data. Vertical distributions of pollutants could be another issue for pollutants with different release heights. Losses of different species during transport, although not fast during our experiment, need to be taken into account as well.

[40] For losses of pollutants through chemical and physical processes, CO has a lifetime much longer (~60 days) than SO_2 and NO_x (~2–3 days); the observed ratios will be higher than the actual emissions. However, the effects of chemical reactions are likely to be small for this study, because of the proximity of our observational site to heavily populated areas and emission sources. Trajectory analysis (Figure 5) suggests that plumes from Beijing could reach Xianghe in just a few hours. In addition, chemical transformation of SO_2 and NO_x during our observation period is limited by relatively cold temperature, low relative humidity, and weak solar radiation. This is supported by the relatively low ozone concentration observed during the experiment. *Dickerson et al.* [2007] estimated the overall removal rate for SO_2, using inventory emission rate and SO_2 profile observed during the aircraft experiment in April 2005 in northern China, and found a SO_2 lifetime of one day or longer. During our ground experiment, the SO_2 lifetime could be even longer with slower photochemical processes. Indeed, a winter experiment in Beijing suggests that by mole fraction, only about 15% of total sulfur (SO_2 and sulfate) exists as sulfate aerosols [*Yao et al.*, 2002]. If we assume the same fraction between sulfate and SO_2 in Xianghe, then the CO/sulfur ratio would be about 30 for west/southwest trajectories, still almost a factor of two higher than the emission inventory value for the area west/southwest of Xianghe.

Table 4. Results of Correlation Analysis for Different Trajectory Groups[a]

	North and Northwest			Southwest and West			Beijing		
	a	b	R^2	a	b	R^2	a	b	R^2
CO/SO_2	33.1	193.6	0.469	36.7	167.5	0.847	41.4	48.4	0.842
CO/NO_x	40.6	64.4	0.525	21.8	335.4	0.758	36.5	−91.6	0.908
NO_x/SO_2	0.71	3.7	0.665	1.47	−3.8	0.832	1.05	5.65	0.775

[a]a, slope (ppbv/ppbv); b, y-intercept.

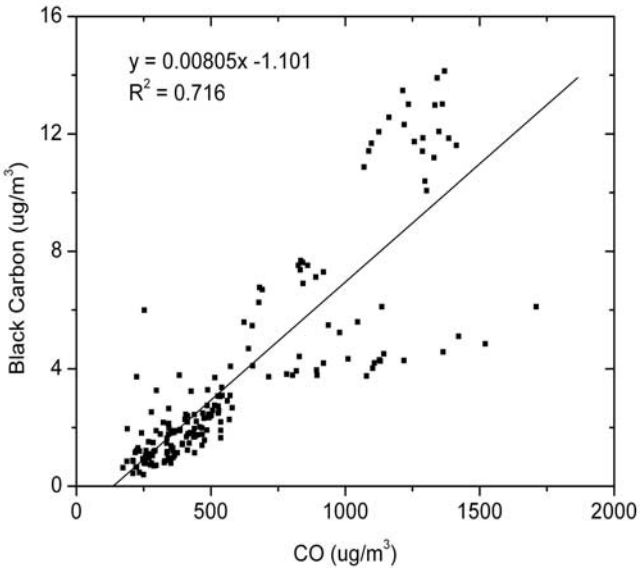

Figure 6. Correlation between 10-min averaged BC and CO concentrations during the afternoon hours (1400–1600 LST) at the Xianghe site (2–26 March 2005).

[41] Surface measurements cannot exactly mirror all emission sources in an area, if different pollutants are emitted at different release heights and thus have different vertical distributions. In China, a considerable part of SO_2 is emitted from large point sources such as power plants, with higher plume height. CO, on the other hand, is largely emitted from numerous surface sources such as automobiles and domestic stoves, although steel mills inject CO at relatively high altitudes. Consequently the CO/SO_2 ratios measured at surface would be higher than inventory values. This sampling bias is partly avoided in our analysis, as we select measurements from local afternoon for comparisons, when vertical mixing within PBL is most vigorous. As a fast test for the influence of pollutant emission heights, we calculated the regional CO/SO_2 inventory ratio with only area sources being considered (i.e., excluding large point sources for CO and SO_2). The surface-source-only ratio for the area west/southwest of Xianghe (37.5–40°N, 114–117°E) is about 20.8 [*Streets et al.*, 2006], about 25% higher than the all-source-ratios (~16.5), but still about 70% lower than observations. Aircraft measurements made over northeastern China (about 600 km northeast of Xianghe) in April 2005 suggest that CO/SO_2 ratios are roughly 45 at about 300 m above ground [*Dickerson et al.*, 2007].

[42] The inventory studies compared here are based on activity data of the year 2000 and 2001, but our experiment was carried out in 2005. Inventory studies estimate emissions for the whole year, while this observation only lasted for less than one month. These inconsistencies further complicate direct comparisons between observations and inventories, although the inventory emissions of CO, SO_2, and NO_x in March are very close to annual averages [*Streets et al.*, 2003] and there is no discernable change in monitored CO/SO_2 ratios in Beijing from 2000 to 2004 (T. Wen, personal communication, 2006). In summary, different spatial and temporal coverages, chemical and physical losses of pollutants, uncertainties in measurements, and uncertainties in emission estimates all contribute to the discrepancies found in the pollutant ratio comparisons. Reducing the gap between field experiment and bottom-up estimates helps improve emission inventories. The better agreement between the new CO inventory for China [*Streets et al.*, 2006] and our measurements reflects an important achievement of TRACE-P field experiment, although significant uncertainties still exist, as revealed in this study. More extensive field experiments over multiple locations and longer period, along with direct emission factor measurements especially for mobile sources and small boilers, may further improve our understanding of pollutant emissions from China.

3.4.4. Black Carbon Emissions

[43] Since CO and BC are both products of inefficient combustion, the correlation between them could provide an estimate of BC emissions. Data (Figure 6) from the afternoon hours (1400–1600 LST) were used to avoid sampling biases at night and to get a more regionally representative ratio. The mass concentration of BC was calculated using PSAP aerosol absorption data and assuming that BC was the only important absorbing aerosol species. The specific absorption coefficient of BC was assumed to be 10 m^2/g at 550 nm, regardless of changes in RH and aerosol size distribution. The value was adopted from *Barnard et al.* [2005], as both experiments were conducted in developing areas with influences from megacities (the Mexico City for *Barnard et al.* [2005] and Beijing for this study). The mass concentration of CO was calculated with the colocated ambient pressure and temperature observations.

[44] The BC/CO ratio obtained in this study is 8.05×10^{-3} ($\mu g/m^3$ BC versus $\mu g/m^3$ CO), lower than observed over the Indian Ocean during INDOEX (12.5×10^{-3} [*Dickerson et al.*, 2002]) and higher than that for the eastern United States (3.4×10^{-3} [*Chen et al.*, 2001]). In spite of the uncertainties associated with sampling and measurements, the different ratios likely reflect differences in energy consumption for these regions. Among the three regions, India probably has the most intense emissions from biomass burning, while the United States has the least contribution from biomass burning. The inefficient combustion of other fuel types and high-emission vehicle fleets in India and China also contributes to the high BC/CO ratios as observed in INDOEX and this study. The complex nature of CO and BC emissions complicates further study of this issue, because of the lack of direct emission profile measurements in both countries. Using the ratio in Figure 6 and the CO emissions estimated by *Streets et al.* [2006], the BC emitted from China for the year 2001 is estimated at ~1300 Gg/yr, in agreement with the inventory (1049 Gg/yr [*Streets et al.*, 2003]). If we assume, as suggested by the observed CO/SO_2 ratios from all afternoon data that the actual CO emissions could be a factor of two higher than given by *Streets et al.* [2006], then the BC emissions could be as high as 2600 Gg/yr. The relative uncertainty of this estimate is large (at least a factor of two) and ill constrained because considerable uncertainties exist in all of the following aspects: BC measurements, applying data from a single location to a much larger area of very diverse sources, and CO emission estimates. Nonetheless, the BC emissions

derived using the bottom-up methods and the observational results are in much better agreement than for India [*Dickerson et al.*, 2002].

4. Conclusions

[45] Simultaneous measurements of CO, SO_2, NO_y, O_3, aerosol scattering coefficients, and aerosol absorption coefficients have been made at Xianghe, a rural site about 70 km southeast of downtown Beijing. Located in a rural area undergoing fast industrialization near more developed mega cities, the Xianghe site provides a useful perspective for the air pollution in China.

[46] During the experiment in March 2005, air pollution at the Xianghe site was generally characterized by high pollutant levels and fast transitions between clean and heavily polluted events. Cold front passages, repeating every 4–5 days during the experiment, are the major mechanism driving these transitions, as they are associated with strong vertical motions and wind shear accompanying the change of air mass. The observed response of air quality to synoptic changes is similar to what has been found in eastern United States. However, in contrast to the eastern United States, northern China is much drier in March, and wet deposition is inefficient in removing pollutants in this region at this time of year. We propose that pollutants are lofted away from the surface during cold front passages, but their exact altitude and fate after uplifting need further investigation. The role of these rain-free cold fronts in pollutant uplift and transport will be further discussed in a companion paper presenting results from the aircraft experiment during the 2005 IFC of EAST-AIRE [*Dickerson et al.*, 2007].

[47] In addition to the synoptic-scale change associated with the cold front passages, we also observed the seasonal trends exhibited by decreases in SO_2 and NO_y and increase in O_3. The driving forces of the observed seasonal changes appear to be two-fold, with nature (increasing ambient temperature, solar radiation and atmospheric instability) and human activities (varying emissions) both playing a role. The observed diurnal cycle of pollutants discloses the diverse nature of the emission sources around the Xianghe site. The pollutant levels are variable in the morning, when wind speed is lower and atmospheric mixing is less intense. During the morning rush hour (0700–0900 LST), the instruments appear to capture more ''local'' and fresh pollutants, while in the afternoon hours (1400–1600 LST) the Xianghe site sees more ''regional'' and well-mixed aged pollutants. This is confirmed by the pollutant ratios obtained via correlation analysis for these two time intervals. Single scattering albedos, derived from the morning and afternoon b_{sp}/b_{ap} ratios, were 0.81 and 0.85 during the experiment, confirming the strong absorbing aerosol properties found from some other measurements made in the eastern part of China [*Bergin et al.*, 2001; *Xu et al.*, 2002, 2003; *Andreae et al.*, 2005]. However, the ground-level values are much lower than the column value ($\sim$0.9) as retrieved from the Cimel Sun photometer measurements made at the same site [*Li et al.*, 2007]. The strongly absorbing aerosols at lower levels could have important impacts on the local radiation budget as well as atmospheric stability. Further work is needed to quantitatively estimate these effects.

[48] Using the CO emission data from *Streets et al.* [2006] and the BC/CO ratio obtained in this experiment, the black carbon emitted from China was estimated to be about 1300 Gg/yr, but could be as high as 2600 Gg/yr. The agreement between the observations and bottom-up studies is better than for India. However, future field experiments in China are important to reduce the large uncertainties in this estimate.

[49] Afternoon pollutant ratios (CO/SO_2, CO/NO_x (NO_y)) were also compared to inventory studies as well as to measurements made in downtown Beijing. With a 36% increase in CO emissions from China, the updated CO inventory by *Streets et al.* [2006] agrees better with our observations than earlier emission inventories [*Streets et al.*, 2003; *Wang et al.*, 2005], although a factor of two difference in CO/SO_2 ratios still exists. CO/NO_x or CO/NO_y ratios derived from this experiment are close to those of Wen et al. (manuscript in preparation, 2007) as well as *Streets et al.* [2003, 2006], but a factor of four higher than *Wang et al.* [2005]. Further analysis suggests that a number of issues could contribute to the difference between observations and inventories, including but not limited to temporal and spatial coverage of measurements, different release heights of pollutants, chemical and physical losses of pollutants, and inventory errors. However, for air from west and southwest, the observation-derived CO/SO_2 ratios are consistently more than 100% higher than the inventory values for the area west and southwest of Xianghe, which is relatively more populated and industrialized/urbanized. The differences in CO/SO_2 and CO/NO_y ratios are even larger for plumes from the grid of downtown Beijing, with the inventory CO/SO_2 ratio for Beijing (12.5) being only about one third of the observed ratio. In situ measurements made in downtown Beijing suggests higher CO/SO_2 ratios (Wen et al., manuscript in preparation, 2007) than our measurements. As discussed in section 3.4, the differences between inventories and observations for the more urbanized and industrialized area west and southwest of Xianghe cannot be totally explained by chemical losses of SO_2 or different emission heights of SO_2 and CO. We also noticed that the inventories tend to give low CO/SO_2 (NO_x) ratios for big cities in China [*Streets et al.*, 2003, 2006]. Such comparisons suggest substantial uncertainties in emissions inventories. While quantitatively evaluating CO or SO_2 emissions for the whole country is not likely with the data set presented here, it is possible that CO emitted from China could still be underestimated (or SO_2 is overestimated or SO_2 emissions have decreased in recent years) by current emission inventory [*Streets et al.*, 2006], since the inventory has difficulty matching the observed CO/SO_2 ratios for regions with strong pollutant emissions (big cities and more populated and industrialized areas). Extensive ambient measurements at multiple locations and altitudes over longer period, as well as direct characterization of emission sources such as mobile sources and small-scale boilers are key to better understanding pollutant emissions from China.

[50] **Acknowledgments.** The EAST-AIRE project was supported by the NASA Radiation Science Program (NNG04GE79G), the National Science Foundation (ATM0412040), the National Science Foundation of China (40250120071), and the Chinese Academy of Sciences (2003-2-9). The authors wish to thank D. Streets and Q. Zhang of Argonne National Laboratory for providing emission inventory data and a lot of helpful

discussions. We also wish to thank the two anonymous reviewers for helping improve the manuscript.

References

Allen, D., K. Pickering, and M. Fox-Rabinovitz (2004), Evaluation of pollutant outflow and CO sources during TRACE-P using model-calculated, aircraft-based, and measurements of pollution in the troposphere (MOPITT)-derived CO concentrations, *J. Geophys. Res.*, *109*, D15S03, doi:10.1029/2003JD004250.

Anderson, T. L., and J. A. Ogren (1998), Determining aerosol radiative properties using the TSI 3563 Integrating Nephelometer, *Aerosol Sci. Technol.*, *29*, 57–69.

Anderson, T. L., et al. (1996), Performance characteristics of a high-sensitivity, three-wavelength, total scatter/backscatter nephelometer, *J. Atmos. Oceanic*, 13,967–13,986.

Andreae, M. O., and P. Merlet (2001), Emissions of trace gases and aerosols from biomass burning, *Global Biogeochem. Cycles*, *15*, 955–966.

Andreae, M. O., O. Schmid, H. Yang, D. Chand, J. Yu, Y. Zhang, and L. Zeng (2005), Aerosol optical and chemical properties in urban Guangzhou, China, *Eos Trans. AGU*, *86*(18), Jt. Assem. Suppl., Abstract A21A-23.

Barnard, J. C., E. I. Kassianov, T. P. Ackerman, S. Frey, K. Johnson, B. Zuberi, L. T. Molina, M. J. Molina, J. S. Gaffney, and N. A. Marley (2005), Measurements of black carbon specific absorption in the Mexico City metropolitan area during the MCMA 2003 field campaign, *Atmos. Chem. Phys. Disc.*, *5*, 4083–4113.

Beijing EPA (2002), Integrated emission standard of boiler pollutants (in Chinese), *DB11/139-2002*, Beijing, China.

Bergin, M. H., et al. (2001), Aerosol radiative, physical, and chemical properties in Beijing during June, 1999, *J. Geophys. Res.*, *106*(D16), 17,969–17,980.

Berntsen, T. K., S. Karlsdóttir, and D. A. Jaffe (1999), Influence of Asian emissions on the composition of air reaching the North Western United States, *Geophys. Res. Lett.*, *26*(14), 2171–2174.

Bond, T. C., T. L. Anderson, and D. Campbell (1999), Calibration and intercomparison of filter-based measurements of visible light absorption by aerosols, *Aerosol Sci. Technol.*, *30*, 582–600.

Brajer, V., and R. W. Mead (2003), Blue skies in Beijing? Looking at the Olympic effect, *J. Environ. Dev.*, *12*(2), 239–263.

Carmichael, G. R., et al. (2003), Evaluating regional emission estimates using the TRACE-P observations, *J. Geophys. Res.*, *108*(D21), 8810, doi:10.1029/2002JD003116.

Chan, C. Y., X. D. Xu, Y. S. Li, K. H. Wong, G. A. Ding, L. Y. Chan, and X. H. Cheng (2005), Characteristics of vertical profiles and sources of PM2.5, PM10 and carbonaceous species in Beijing, *Atmos. Environ.*, *39*, 5113–5124.

Charlson, R. J., S. E. Schwartz, J. M. Hales, R. D. Cess, J. A. Coakley, J. E. Hansen, and D. J. Hofmann (1992), Climate forcing by anthropogenic aerosols, *Science*, *255*, 423–430.

Chen, L.-W. A., B. G. Doddridge, R. R. Dickerson, J. C. Chow, P. K. Mueller, J. Quinn, and W. A. Butler (2001), Seasonal variations in elemental carbon aerosol, carbon monoxide and sulfur dioxide: Implications for sources, *Geophys. Res. Lett.*, *28*(9), 1711–1714.

Crutzen, P. J., and M. O. Andreae (1990), Biomass burning in the tropics: Impact on atmospheric chemistry and biogeochemical cycles, *Science*, *250*, 1669–1678.

Delene, D. J., and J. A. Ogren (2002), Variability of aerosol optical properties at four North American surface monitoring sites, *J. Atmos. Sci.*, *59*, 1135–1150.

Dickerson, R. R., and A. C. Delany (1988), Modification of a commercial gas filter correlation CO detector for enhanced sensitivity, *J. Atmos. Oceanic Technol.*, *5*, 424–5431.

Dickerson, R. R., A. C. Delany, and A. F. Wartburg (1984), Further modification of a commercial NO_x detector for high sensitivity, *Rev. Sci. Instrum.*, *55*(12), 1995–1998.

Dickerson, R. R., M. O. Andreae, T. Campos, O. L. Mayol-Bracero, C. Neusuess, and D. G. Streets (2002), Analysis of black carbon and carbon monoxide observed over the Indian Ocean: Implications for emissions and photochemistry, *J. Geophys. Res.*, *107*(D19), 8017, doi:10.1029/2001JD000501.

Dickerson, R. R., et al. (2007), Aircraft observations of dust and pollutants over NE China: Insight into the meteorological mechanisms of long-range transport, *J. Geophys. Res.*, doi:10.1029/2007JD008999, in press.

Draxler, R. R., and G. D. Rolph (2003), HYSPLIT (HYbrid Single-Particle Lagrangian Integrated Trajectory) model access via NOAA ARL READY Website, htttp://www.arl.noaa.gov/ready/hysplit4.html, NOAA Air Resour. Lab., Silver Spring, Md.

Fehsenfeld, F. C., et al. (1987), A ground-based intercomparison of NO, NO_x, NO_y measurement techniques, *J. Geophys. Res.*, *92*(12), 14,710–14,722.

Guttikunda, S. K., Y. Tang, G. R. Carmichael, G. Kurata, L. Pan, D. G. Streets, J.-H. Woo, N. Thongboonchoo, and A. Fried (2005), Impacts of Asian megacity emissions on regional air quality during spring 2001, *J. Geophys. Res.*, *110*, D20301, doi:10.1029/2004JD004921.

Hao, J., and L. Wang (2005), Improving urban air quality in China: Beijing case study, *J. Air Waste Manage. Assoc.*, *55*, 1298–1305.

He, B. S., and C. H. Chen (2002), Energy ecological efficiency of coal fired plant in China, *Energy Convers. Manage.*, *43*, 2553–2567.

He, K., F. Yang, Y. Ma, Q. Zhang, X. Yao, C. K. Chan, S. Cadle, T. Chan, and P. Mulawa (2001), The characteristics of $PM_{2.5}$ in Beijing, China, *Atmos. Environ.*, *35*, 4959–4970.

Heald, C. L., D. J. Jacob, D. B. A. Jones, P. I. Palmer, J. A. Logan, D. G. Streets, G. W. Sachse, J. C. Gille, R. N. Hoffman, and T. Nehrkorn (2004), Comparative inverse analysis of satellite (MOPITT) and aircraft (TRACE-P) observations to estimate Asian sources of carbon monoxide, *J. Geophys. Res.*, *109*, D23306, doi:10.1029/2004JD005185.

Hoell, J. M., D. D. Davis, S. C. Liu, R. E. Newell, H. Akimoto, R. J. McNeal, and R. J. Bendura (1997), The Pacific Exploratory Mission-West Phase B: February–March, 1994, *J. Geophys. Res.*, *102*(D23), 28,223–28,240.

Huang, Y., R. E. Dickinson, and W. L. Chameides (2006), Impact of aerosol indirect effect on surface temperature over East Asia, *Proc. Natl. Acad. Sci. U. S. A.*, *103*, 4371–4376.

Huebert, B. J., T. Bates, P. B. Russell, G. Shi, Y. J. Kim, K. Kawamura, G. Carmichael, and T. Nakajima (2003), An overview of ACE-Asia: Strategies for quantifying the relationships between Asian aerosols and their climatic impacts, *J. Geophys. Res.*, *108*(D23), 8633, doi:10.1029/2003JD003550.

Husar, R. B., et al. (2001), Asian dust events of April 1998, *J. Geophys. Res.*, *106*(D16), 18,317–18,330.

Jacob, D. J., J. H. Crawford, M. M. Kleb, V. S. Connors, R. J. Bendura, J. L. Raper, G. W. Sachse, J. C. Gille, L. Emmons, and C. L. Heald (2003), Transport and Chemical Evolution over the Pacific (TRACE-P) aircraft mission: Design, execution, and first results, *J. Geophys. Res.*, *108*(D20), 9000, doi:10.1029/2002JD003276.

Jaffe, D. A., et al. (1999), Transport of Asian air pollution to North America, *Geophys. Res. Lett.*, *26*, 711–714.

Jaffe, D., H. Price, D. Parrish, A. Goldstein, and J. Harris (2003), Increasing background ozone during spring on the west coast of North America, *Geophys. Res. Lett.*, *30*(12), 1613, doi:10.1029/2003GL017024.

Jeong, M.-J., Z. Li, E. Andrews, and S.-C. Tsay (2007), Effect of aerosol humidification on the column aerosol optical thickness over the Atmospheric Radiation Measurement Southern Great Plains site, *J. Geophys. Res.*, *112*, D10202, doi:10.1029/2006JD007176.

Lau, K.-M., K.-M. Kim, and N.-C. Hsu (2005), Observational evidence of effects of absorbing aerosols on seasonal-to-interannual anomalies of the Asian monsoon, *CLIVAR Exch.*, *10*(3), 7–9.

Li, Z., et al. (2007), Aerosol optical properties and their radiative effects in northern China, *J. Geophys. Res.*, doi:10.1029/2006JD007382, in press.

Luke, W. T. (1997), Evaluation of a commercial pulsed fluorescence detector for the measurement of low-level SO_2 concentrations during the Gas-Phase Sulfur Intercomparison Experiment, *J. Geophys. Res.*, *102*, 16,255–16,265.

Mari, C., M. J. Evans, P. I. Palmer, D. J. Jacob, and G. W. Sachse (2004), Export of Asian pollution during two cold front episodes of the TRACE-P experiment, *J. Geophys. Res.*, *109*, D15S17, doi:10.1029/2003JD004307.

Menon, S., J. Hansen, L. Nazarenko, and Y. Luo (2002), Climate effects of black carbon aerosols in China and India, *Science*, *297*, 2250–2253.

Novelli, P. C., K. A. Masarie, and P. M. Lang (1998), Distributions and recent changes of carbon monoxide in the lower troposphere, *J. Geophys. Res.*, *103*, 19,015–19,033.

Parrish, D. D., Y. Kondo, O. R. Cooper, C. A. Brock, D. A. Jaffe, M. Trainer, T. Ogawa, G. Hübler, and F. C. Fehsenfeld (2004), Intercontinental transport and chemical transformation 2002 (ITCT 2K2) and pacific exploration of Asian continental emission (PEACE) experiments: An overview of the 2002 winter and spring intensives, *J. Geophys. Res.*, *109*, D23S01, doi:10.1029/2004JD004980.

Prospero, J. M., D. L. Savoie, and R. Arimoto (2003), Long-term record of nss-sulfate and nitrate in aerosols on Midway Island, 1981–2000: Evidence of increased (now decreasing?) anthropogenic emissions from Asia, *J. Geophys. Res.*, *108*(D1), 4019, doi:10.1029/2001JD001524.

Richter, A., J. P. Burrows, H. Nüß, C. Granier, and U. Niemeier (2005), Increase in tropospheric nitrogen dioxide over China observed from space, *Nature*, *437*, 129–132.

Seinfeld, J. H., and S. N. Pandis (1998), *Atmospheric Chemistry and Physics: From Air Pollution to Climate Change*, 1326 pp., John Wiley, New York.

Stehr, J. W., R. R. Dickerson, K. A. Hallock-Waters, B. G. Doddridge, and D. Kirk (2000), Observations of NO_y, CO, and SO_2 and the origin of reactive nitrogen in the eastern United States, *J. Geophys. Res.*, *105*(D3), 3553–3563.

Streets, D. G., and K. Aunan (2005), The importance of China's household sector for black carbon emissions, *Geophys. Res. Lett.*, *32*, L12708, doi:10.1029/2005GL022960.

Streets, D. G., and S. T. Waldhoff (2000), Present and future emissions of air pollutants in China: SO_2, NO_x, and CO, *Atmos. Environ.*, *34*, 363–374.

Streets, D. G., et al. (2003), An inventory of gaseous and primary aerosol emissions in Asia in the year 2000, *J. Geophys. Res.*, *108*(D21), 8809, doi:10.1029/2002JD003093.

Streets, D. G., Q. Zhang, L. Wang, K. He, J. Hao, Y. Wu, Y. Tang, and G. R. Carmichael (2006), Revisiting China's CO emissions after the Transport and Chemical Evolution over the Pacific (TRACE-P) mission: Synthesis of inventories, atmospheric modeling, and observations, *J. Geophys. Res.*, *111*, D14306, doi:10.1029/2006JD007118.

Sun, Y., G. Zhuang, Y. Wang, X. Zhao, J. Li, Z. Wang, and Z. An (2005), Chemical composition of dust storms in Beijing and implications for the mixing of mineral aerosol with pollution on the pathway, *J. Geophys. Res.*, *110*, D24209, doi:10.1029/2005JD006054.

Tan, Q., W. L. Chameides, D. Streets, T. Wang, J. Xu, M. Bergin, and J. Woo (2004), An evaluation of TRACE-P emission inventories from China using a regional model and chemical measurements, *J. Geophys. Res.*, *109*, D22305, doi:10.1029/2004JD005071.

Taubman, B. F., L. T. Marufu, C. A. Piety, B. G. Doddridge, J. W. Stehr, and R. R. Dickerson (2004), Airborne characterization of the chemical, optical, and meteorological properties, and origins of a combined ozone-haze episode over the Eastern United States, *J. Atmos. Sci.*, *61*, 1781–1793.

Virkkula, A., N. C. Ahlquist, D. S. Covert, W. P. Arnott, P. J. Sheridan, P. K. Quinn, and D. J. Coffman (2005), Modification, calibration and a field test of an instrument for measuring light absorption by particles, *Aerosol Sci. Technol.*, *39*, 68–83.

Wang, T., T. F. Cheung, Y. S. Li, X. M. Yu, and D. R. Blake (2002), Emission characteristics of CO, NO_x, SO_2 and indications of biomass burning observed at a rural site in eastern China, *J. Geophys. Res.*, *107*(D12), 4157, doi:10.1029/2001JD000724.

Wang, T., et al. (2004), Relationships of trace gases and aerosols and the emission characteristics at Lin'an, a rural site in eastern China, during spring 2001, *J. Geophys. Res.*, *109*, D19S05, doi:10.1029/2003JD004119.

Wang, X., D. L. Mauzerall, Y. Hu, A. G. Russell, E. D. Larson, J.-H. Woo, D. G. Streets, and A. Guenther (2005), A high-resolution emission inventory for eastern China in 2000 and three scenarios for 2020, *Atmos. Environ.*, *39*, 5917–5933.

Wang, Y., Y. Choi, T. Zeng, B. Ridley, N. Blake, D. Blake, and F. Flocke (2006), Late-spring increase of trans-Pacific pollution transport in the upper troposphere, *Geophys. Res. Lett.*, *33*, L01811, doi:10.1029/2005GL024975.

World Bank (2004), *Clean Development Mechanism in China: Taking a Proactive and Sustainable Approach*, 2nd ed., 170 pp., Washington, D. C.

World Health Organization (2001), *Environment and People's Health in China*, 76 pp., Geneva, Switzerland.

Xu, J., M. H. Bergin, X. Yu, G. Liu, J. Zhao, C. M. Carrico, and K. Baumann (2002), Measurement of aerosol chemical, physical, and radiative properties in the Yangtze delta region of China, *Atmos. Environ.*, *36*, 161–173.

Xu, J., M. H. Bergin, R. Greenwald, and P. B. Russell (2003), Direct aerosol radiative forcing in the Yangtze delta region of China: Observation and model estimation, *J. Geophys. Res.*, *108*(D2), 4060, doi:10.1029/2002JD002550.

Xu, Q. (2001), Abrupt change of the mid-summer climate in central east China by the influence of atmospheric pollution, *Atmos. Environ.*, *35*, 5029–5040.

Yang, F., K. He, B. Ye, X. Chen, L. Cha, S. H. Cadle, T. Chan, and P. A. Mulawa (2005), One-year record of organic and elemental carbon in fine particles in downtown Beijing and Shanghai, *Atmos. Chem. Phys.*, *5*, 1449–1457.

Yao, X., C. K. Chan, M. Fang, S. Cadle, T. Chan, P. Mulawa, K. He, and B. Ye (2002), The water-soluble ionic composition of PM2.5 in Shanghai and Beijing, *China, Atmos. Environ.*, *36*, 4223–4234.

Zhang, J., K. R. Smith, R. Uma, Y. Ma, V. V. N. Kishore, K. Lata, M. A. K. Khalil, R. A. Rasmussen, and S. T. Thorneloe (1999), Carbon monoxide from cookstoves in developing countries: 1. Emission factors, *Chemosphere*, *1*, 353–366.

Zhang, M., I. Uno, Y. Yoshida, Y. Xu, Z. Wang, H. Akimoto, T. T. Quinn, A. Bandy, and B. Blomquist (2004), Transport and transformation of sulfur compounds over East Asia during the TRACE-P and ACE-Asia campaigns, *Atmos. Environ.*, *38*(40), 6947–6959.

Zheng, M., L. G. Salmon, J. J. Schauer, L. Zeng, C. S. Kiang, Y. Zhang, and G. R. Cass (2005), Seasonal trends in PM2.5 source contributions in Beijing, *China, Atmos. Environ.*, *39*, 3967–3976.

H. Chen, P. Wang, Y. Wang, and T. Wen, Institute of Atmospheric Physics, Chinese Academy of Sciences, Beijing 100029, China.

R. R. Dickerson, C. Li, Z. Li, L. T. Marufu, and J. W. Stehr, Department of Atmospheric and Oceanic Science, University of Maryland, College Park, MD 20742, USA. (russ@atmos.umd.edu)